The Antiangiogenic Effects of Gold Nanoparticles on Experimental Choroidal Neovascularization in Mice

Young-Jung Roh,[1] Chang Rae Rho,[1,2] Won-Kyung Cho,[1,2] and Seungbum Kang[1,2]

[1]Department of Ophthalmology and Visual Science, College of Medicine, The Catholic University of Korea, Seoul, Republic of Korea
[2]Clinical Research Institute, College of Medicine, Daejeon St. Mary's Hospital, The Catholic University of Korea, Daejeon, Republic of Korea

Correspondence: Seungbum Kang, Department of Ophthalmology and Visual Science, College of Medicine, Daejeon St. Mary's Hospital, The Catholic University of Korea, 64 Daeheung-ro, Jung-gu, Daejeon 301-012, Republic of Korea; john0730@catholic.ac.kr.

Submitted: April 17, 2016
Accepted: November 3, 2016

Citation: Roh Y-J, Rho CR, Cho W-K, Kang S. The antiangiogenic effects of gold nanoparticles on experimental choroidal neovascularization in mice. *Invest Ophthalmol Vis Sci.* 2016;57:6561–6567. DOI:10.1167/iovs.16-19754

Purpose. The purpose of this study was to evaluate the antiangiogenic effect of gold nanoparticles (AuNPs) on experimental choroidal neovascularization (CNV) in mice.

Methods. Choroidal neovascularization was induced by rupturing the Bruch's membrane using laser photocoagulation in C57BL/6 mice. The following day, intravitreal injections of AuNPs were administered. The control group received PBS injection of the same volume. Two weeks after laser injury, CNV lesions were evaluated by examination of choroidal flat-mounts using fluorescein-labeled dextran and immunofluorescence staining with isolectin B4. The effects of AuNPs on endothelial cell tube formation, proliferation, and cytotoxicity were evaluated using human umbilical vein endothelial cells (HUVECs) or human RPE cells. The activity of extracellular signal–regulated kinase (ERK)1/2, protein kinase B (Akt), and focal adhesion kinase (FAK) signaling pathways was also analyzed.

Results. The AuNPs reduced the extent of CNV. Mice treated with intravitreal AuNPs injections exhibited a 67.9% reduction in the extent of CNV lesions compared with the control group ($P < 0.001$). The size of the isolectin B4-labeled area was also significantly smaller in AuNP-treated groups compared with the control group ($P < 0.001$). Gold nanoparticles decreased vascular endothelial growth factor–induced HUVEC tube formation and proliferation but showed no RPE cell toxicity with the treatment doses administered. The phosphorylation of ERK1/2, Akt, and FAK in HUVECs was suppressed by AuNPs.

Conclusions. Gold nanoparticles can inhibit laser-induced CNV in mice and may have an indication for the treatment of CNV.

Keywords: age-related macular degeneration, angiogenesis, choroidal neovascularization, gold nanoparticles

Neovascular AMD, with development of choroidal neovascularization (CNV), accounts for a significant amount of irreversible vision loss.[1] Choroidal neovascularization is characterized by the growth of abnormal blood vessels from choriocapillaries and tends to leak blood and fluid that damages photoreceptor cells. It can ultimately evolve into fibrovascular scar tissue, causing permanent vision loss.[2]

The exact pathogenesis underlying CNV development has not been fully elucidated. However, VEGF is considered a critical factor in the pathogenesis of CNV.[3] During normal conditions, angiogenic processes are tightly regulated by a balance of pro- and antiangiogenic growth factors. However, in pathologic conditions, this balance is disrupted, and proangiogenic growth factors are overproduced and interact with their respective receptors, thereby triggering angiogenic signaling cascades.[4] Among the various growth factors involved in angiogenesis, VEGF has been implicated as the major contributor to physiologic and pathologic angiogenesis.[5,6] Binding of VEGF to VEGF receptor-2 (VEGFR-2) activates several signal transduction pathways, leading to increased proliferation, survival, permeability, and migration of endothelial cells.[7] Overactivation of the VEGF–VEGFR2 signaling axis has been proven to significantly contribute to the CNV formation and progression.[8] Therefore, VEGF signal interference is a promising methodology to inhibit CNV progression.[5]

Recent advances in nanotechnology have provided new therapeutic possibilities using nanoparticles. Gold nanoparticles (AuNPs) are the preferred type of nanoparticles for nanomedicine because of their low cytotoxicity; ease of making surface modifications with thiol-containing molecules; ease of conjugating to wide range of biomolecules, such as amino acids, proteins, enzymes, and DNA; and high optical extinction coefficients.[9–11]

Previous studies have reported that AuNPs exert antiangiogenic effects by interacting with the heparin-binding domain of VEGF.[12] Furthermore, AuNPs are also reported to suppress VEGFR-2 activation.[13] Gold nanoparticles have been explored with respect to their efficacy in the treatment of various angiogenesis-related diseases and have been used to suppress progression in various tumor models and in a retinopathy of a prematurity animal model.[13,14]

Therefore, in the present study, the antiangiogenic effects and molecular mechanisms of AuNPs on VEGF-induced angiogenesis were investigated. Moreover, the angiogenic effects of AuNPs in an experimental CNV model were evaluated to determine their potential as a treatment for CNV developing secondary to neovascular AMD.

This work is licensed under a Creative Commons Attribution-NonCommercial-NoDerivatives 4.0 International License.

Downloaded from iovs.arvojournals.org on 01/20/2022

Materials and Methods

Animals and Cell Culture

A total of 40 C57BL/6 mice (age, 8–9 weeks; weight, 20–22 g) were used in this experimental study. Only male mice were used because of the concern that hormonal cycles in female mice may affect the experiments. All animal studies were reviewed and approved by the Institutional Animal Care and Use Committee of the College of Medicine, Catholic University of Korea. All mice were handled in accordance with the ARVO Statement for the Use of Animals in Ophthalmic and Vision Research. Human umbilical vein endothelial cells (HUVECs) were purchased from Gibco-Life Technologies (Carlsbad, CA, USA) and cultured in medium 200 (Gibco-Life Technologies) supplemented with Low Serum Growth Supplement (Gibco-Life Technologies) in a 37°C incubator under a humidified atmosphere containing 5% CO_2. Human umbilical vein endothelial cells were used at passages 4–6. The RPE cell line (ARPE-19) was obtained from American Type Culture Collection (Manassas, VA, USA). ARPE-19 cells were routinely maintained in Dulbecco's Modified Eagle's Medium/Nutrient Mixture F-12 (DMEM/F12; Gibco-Life Technologies), supplemented with 10% fetal bovine serum (Gibco-Life Technologies) and penicillin/streptomycin (1:100) in a humidified incubator at 37°C and 5% CO_2. ARPE-19 cells from passages 18 through 22 were used in the experiments. Gold nanoparticles (size, 20 nm; surface charge, neutral) were purchased from Sigma-Aldrich Corp. (St. Louis, MO, USA). Different concentrations of AuNPs or VEGF (20 ng/mL; Sigma-Aldrich Corp.) treatment were administered to cultured cells.

Endothelial Cell Tube Formation Assay

An endothelial cell tube formation assay was performed using a kit (BD BioCoat; BD Biosciences, Bedford, MA, USA). Briefly, HUVECs (1×10^5 cells) were seeded onto Matrigel in a humidified 37°C, 5% CO_2 incubator. The cells were cultured in the presence of VEGF (20 ng/mL) or different concentrations of AuNPs (0.1, 1, and 10 μM) for 18 hours. Human umbilical vein endothelial cells were labeled with CellTracker Red CMTPX fluorescent dye (Molecular Probes, Inc., Eugene, OR, USA) and incubated for 20 minutes prior to imaging at 40× magnification. Tube formation was observed by fluorescence microscopy (Eclipse TE300; Nikon, Tokyo, Japan). Quantification of the extent of tube formation was achieved by pixel analysis of the tube formation area as described previously.[15] The pixel numbers in five different areas were counted, and an average value was determined for each sample. The control tube formation was defined as 100%, and percentage increase or decrease in tube formation relative to the control was calculated.

Western Blot Analysis

Standard western blot method was used in this study. Briefly, HUVECs were serum-starved overnight and then treated with VEGF (20 ng/mL) in the presence or absence of AuNPs (10 μM). After 15, 30, and 60 minutes, the cells were harvested and lysed in lysis buffer (Pro-prep Protein Extraction Solution; iNtRON Biotechnology, Sungnam, Korea). Cell lysates were centrifuged at 15,700*g* for 15 minutes at 4°C, and the supernatants were collected to determine the protein concentrations using the bicinchoninic acid protein assay. Equal amounts of protein were electrophoresed on 10% sodium dodecyl sulfate–polyacrylamide gels and transferred electrophoretically onto nitrocellulose membranes (Bio-Rad, Hercules, CA, USA). After blocking, the membranes were incubated overnight at 4°C with appropriate antibodies. Antibodies against the following proteins were used in this study: anti–phospho-extracellular signal–regulated kinases (ERK)1/2 (Cell Signaling, Danvers, MA, USA), anti-ERK1/2 (Cell Signaling), anti–phospho-protein kinase B (Akt) (Cell Signaling), anti-Akt (Cell Signaling), anti–phospho-focal adhesion kinase (FAK) (Cell Signaling), anti-FAK (Cell Signaling), and β-actin. Band intensities were quantified using a molecular imaging system (Molecular Imager ChemiDoc XRS+; Bio-Rad) and expressed in arbitrary units. The expression levels of phosphorylated ERK1/2, AKT, and FAK were normalized to those of total ERK1/2, AKT, and FAK, respectively.

3-(4,5-Dimethylthiazol-2-yl)-2,5-Diphenyl Tetrazolium Bromide Assay

The 3-(4,5-Dimethylthiazol-2-yl)-2,5-diphenyl tetrazolium bromide (MTT) assay was used to verify the effect of AuNPs on HUVEC proliferation. Human umbilical vein endothelial cells (1×10^5 cells per well) were plated in a 96-well plate. Cells were treated with VEGF (20 ng/mL) alone or cotreated with different concentrations of AuNPs (0.1, 1.0, and 10 μM), and further incubated for 48 hours. Next, cells were incubated with 10 μL MTT solution for 4 hours at 37°C. Absorbance was measured at 450 nm using a microplate reader (model 680; Bio-Rad). All experiments were performed in triplicate. The absorbance values are expressed as a percentage of controls, which represented 100% cell proliferation.

Flow Cytometry

ARPE-19 cells (2×10^5 cells) were treated with different concentrations of AuNPs (0.1, 1.0, and 10 μM) and further incubated for 24 hours. Next, cytotoxicity was quantified by fluorescence-activated cell sorting (FACS) using propidium iodide (PI) and annexin V. After incubating with different doses of AuNPs, ARPE-19 cells were detached with trypsin-EDTA, resuspended in fresh culture medium, and stained with PI and annexin V (BD Biosciences, San Jose, CA, USA). Both early (annexin V^+/PI^-) and late (annexin V^+/PI^+) apoptotic ARPE-19 cells were sorted by FACS (BD FACSCanto II flow cytometry; BD Biosciences). Propidium iodide–positive and annexin V–positive cells were quantified after gating using forward and side scattering. The results are expressed as the percentage of PI- and annexin V–stained cells. All experiments were performed in triplicate.

Animal Model of CNV

Experimental CNV was created by laser photocoagulation, as described elsewhere.[16] Briefly, after general anesthesia was induced via an intraperitoneal injection of 30 mg zolazepam (Zoletil; Virbac, Carros, France) and 10 mg xylazine hydrochloride (Rompun; Bayer, Leuverkeusen, Germany) per kilogram of body weight, laser-induced rupture of Bruch's membrane was performed on both eyes. Five laser spots were created per eye and delivered by slit lamp (SL120; Carl Zeiss Meditec, Jena, Germany). The laser pulses were from green laser (wavelength, 532 nm; Visulas 532; Carl Zeiss Meditec). The laser parameters were as follows: spot diameter, 100 μm; intensity, 200 mW; and duration, 0.1 second. Only mice that developed cavitation bubbles, indicating Bruch's membrane rupture, were included in the study. Laser spots with elongated shape, subretinal hemorrhage, and bridging CNV complex were excluded for analysis.

Investigative Ophthalmology & Visual Science

Downloaded from iovs.arvojournals.org on 01/20/2022

Intravitreal Injection

Under general anesthesia, mouse pupils were dilated with 0.5% tropicamide and 0.5% phenylephrine (Mydrin-P; Santen Pharmaceutical Co., Osaka, Japan). Gold nanoparticles (20 nm, 10 μM) or PBS as a control was injected into the vitreous cavity in a total volume of 1 μL with a 33-gauge micro syringe (Hamilton Company, Reno, NV, USA) through the limbus. The injection tip of the syringe in the vitreous cavity was properly placed after visualization under a microscope. We confirmed the movement of injected solution in vitreous cavity during the injection of ruby red-colored AuNPs (Supplementary Video S1). Mice with traumatic lens injury in either the treatment or the control eye were excluded from the study and not included in the statistical analysis. Injections for both groups were performed the day after the laser procedures. Topical levofloxacin eye drops (Oculevo; Samil, Seoul, Korea) were applied to the eyes of each mouse daily for 3 days to minimize the risk of infection after the intravitreal injection.

Preparation of Choroidal Flat Mounts

Twenty mice were randomly divided into two groups: AuNPs treated ($n = 10$) and PBS treated ($n = 10$). One day after laser photocoagulation, intravitreal injection of AuNPs or PBS was performed. Fourteen days after laser injury, mice in each group were anesthetized and perfused through the left ventricle with 1.0 mL PBS containing 25 mg fluorescein isothiocyanate-dextran (molecular weight, 2×10^6 kDa; Sigma-Aldrich Corp.), as described previously.[16,17] Eyes were enucleated and fixed in 4% paraformaldehyde for 1 hour. Retinal pigment epithelium–choroid–sclera eyecups were prepared after hemisecting the eye, with total removal of the lens, vitreous body, and retina. Retinal pigment epithelium–choroid–sclera eyecups were flattened by the creation of four or five radial incisions, from the edge to the equator, and flat-mounted in aquamount with the RPE side facing up. The optical section that shows the largest diameters of the CNV lesion on the flat mounts was measured by scanning laser confocal microscopy (LSM5 live configuration Variotwo VRGB; Carl Zeiss Meditec). Choroidal neovascularization images were digitized using an image capture and analysis program (LSM Image Browser; Zeiss), and data were quantified using the same program. The size of CNV lesions stained with green color was measured by masked two readers (YJR and SBK).

Choroidal Neovascularization Immunofluorescence Staining

Twenty mice were randomly divided into two groups: AuNP-treated mice ($n = 10$) and PBS-treated mice ($n = 10$). Intraviteal injections of AuNPs or PBS were performed 1 day after laser photocoagulation. Two weeks later, the eyes from mice in both groups were enucleated and fixed in 4% paraformaldehyde for 1 hour. Previously described immunofluorescence staining techniques were used to label endothelial cells within CNV lesions.[17] Briefly, the cornea, lens, and vitreous were removed. Next, the retina was gently peeled and separated from the optic disc. The remaining eyecups were rinsed in blocking solution containing 0.5% BSA and 0.2% polysorbate 20 (Tween 20; Sigma-Aldrich Corp.) diluted in PBS and incubated overnight at 4°C with a 1:1000 dilution of a 10 mg/mL solution of 4,6-diamidino-2-phenylindole (DAPI) and a 1:50 dilution of a 1 g/L solution of isolectin B4 conjugated with Alexa Fluor 568 (Molecular Probes, Inc.). The eyecups were washed with cold PBS and flat-mounted. Images were taken using a camera equipped with a fluorescent microscope (Eclipse TE300; Nikon, Tokyo, Japan) and evaluated with image analysis software (NIS Elements BR; Nikon). The fluorescence levels of the CNV lesions are expressed in arbitrary units.

Statistical Analysis

Unless indicated otherwise, data are expressed as means ± SDs. The CNV lesion areas identified using both fluorescein isothiocyanate-dextran perfusion and isolectin B4 were evaluated with unpaired *t*-test. The MTT assay and endothelial tube formation were separately performed three times and were analyzed using an unpaired *t*-test. $P < 0.05$ was considered statistically significant. SPSS version 17.0 (IBM Corp., Armonk, NY, USA) was used for statistical analysis.

Results

Inhibition of HUVEC Tube Formation by AuNPs

As shown in Figure 1A, VEGF treatment led to the formation of capillary-like structures in HUVECs cultured on the Matrigel surface at a 1.6-fold greater level than the control. However, AuNP treatment significantly suppressed the extent of VEGF-induced tube formation in a concentration-dependent manner. Compared with the extent of VEGF-induced tube formation, the extent of HUVEC capillary-like networks was decreased by 47.1%, 63.0%, and 72.6% on treatment with 0.1, 1, and 10 μM AuNPs, respectively (Fig. 1B).

Suppression of VEGF-Induced HUVEC Proliferation by AuNPs

The effects of AuNPs on HUVEC proliferation were tested by the MTT assay. Vascular endothelial growth factor increased the proliferation of HUVECs by 1.45-fold compared with the control. However, cotreatment with AuNPs significantly inhibited VEGF-mediated HUVEC proliferation ($P < 0.05$; Fig. 2).

Flow Cytometry Assay Showed No AuNP Cytotoxicity

Fluorescence-activated cell sorting analysis was used to test ARPE-19 cell apoptosis. ARPE-19 cell cultures with different concentrations of AuNPs did not increase the proportion of either annexin V^+/PI^- or annexin V^+/PI^+ cells. The proportion of annexin V^+/PI^- cells were 0.1% in the control, 0.0% in the 0.1 μM, 0.1% in the 1.0 μM, and 0.0% in the 10 μM AuNPs-treated ARPE-19 cells. The proportion of annexin V^+/PI^+ cells were 1.0%, 0.3%, 0.3%, and 0.3% in the control and 0.1, 1.0, and 10 μM AuNP-treated ARPE-19 cells, respectively. Thus, AuNPs, at least up to 10 μM, exert no cytotoxic effects on ARPE-19 cells, as shown by flow cytometry (Fig. 3).

Gold Nanoparticles Suppressed VEGF-Induced Phosphorylation of ERK1/2, Akt, and FAK

During angiogenesis, phosphorylation of ERK1/2, Akt, and FAK is necessary for triggering proliferation, survival, and migration, respectively, of endothelial cells. Therefore, we examined the effect of AuNPs on the VEGF-induced phosphorylation of ERK1/2 (p-ERK1/2), Akt (p-Akt), and FAK (p-FAK) using HUVECs. Vascular endothelial growth factor alone (20 ng/mL) significantly increased the phosphorylation of ERK1/2, Akt, and FAK at 15, 30, and 60 minutes. However, pretreatment with AuNPs (10 μM) significantly suppressed VEGF-induced phosphorylation of ERK1/2, Akt, and FAK at all time points tested (15, 30, and 60 minutes; Fig. 4).

Investigative Ophthalmology & Visual Science

Downloaded from iovs.arvojournals.org on 01/20/2022

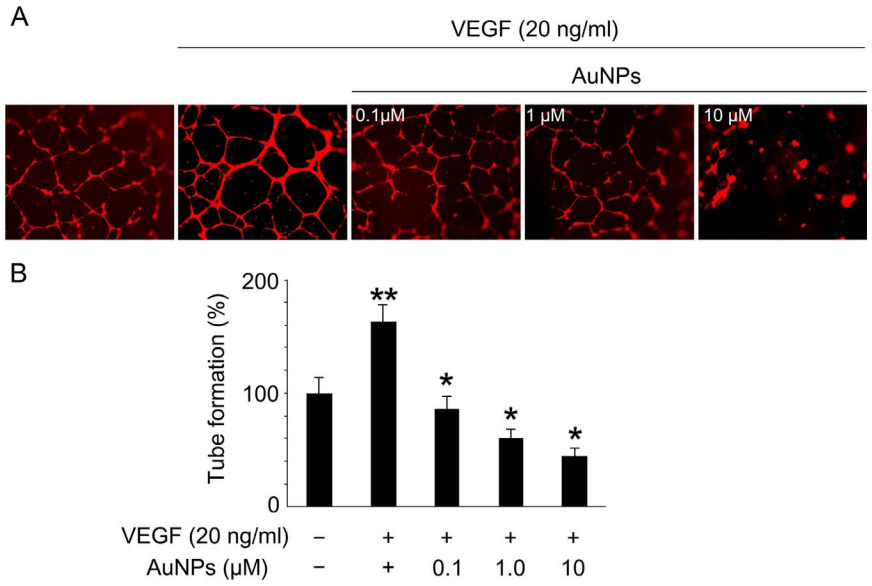

Figure 1. Gold nanoparticles inhibited VEGF-induced HUVEC tube formation. (**A**) Human umbilical vein endothelial cells were seeded and grown on Matrigel for 18 hours at 37°C in 5% CO_2. Human umbilical vein endothelial cells were supplemented with VEGF (20 ng/mL) plus the indicated concentrations of AuNPs (0.1, 1.0, and 10 μM). Untreated HUVECs served as controls. Representative pictures of HUVECs plated on Matrigel were selected from three independent experiments. (**B**) Quantitative analysis of the stained tube-like structures was performed. The basal tube formation of HUVECs without both VEGF and AuNPs was normalized to 100%. Data show the percentage change in tube formation compared with the control. $^{**}P < 0.05$ versus basal tube formation (control); $^{*}P < 0.05$ versus VEGF-induced HUVEC tube formation.

Inhibition of Laser-Induced CNV by Intravitreal AuNP Injection

Similar to previous safety report of 10 μM AuNPs,[13] the concentration of 10 μM AuNPs was used for intravitreal injection. Ninety-three (AuNP-treated mice) and 92 (PBS-treated mice) laser spots out of the respective applied 100 laser spots were evaluated for CNV lesions. Representative images of choroidal flat-mount preparations from intravitreal AuNP-injected and PBS-injected mice are shown in Figures 5A and 5B. An analysis of choroidal flat mounts revealed that intravitreal AuNP injections suppressed laser-induced CNV development. The mean CNV area per lesion was 8400.8 ± 6405.0 μm² in the AuNP-treated group and 26,160.9 ± 9609.9 μm² in the PBS-treated group, with the former representing a 67.9% reduction in CNV growth. Statistically significant differences were evident between the two groups ($P < 0.001$). Choroidal neovascularization areas obtained from choroidal flat-mount preparations are displayed using boxplots in Figure 5C.

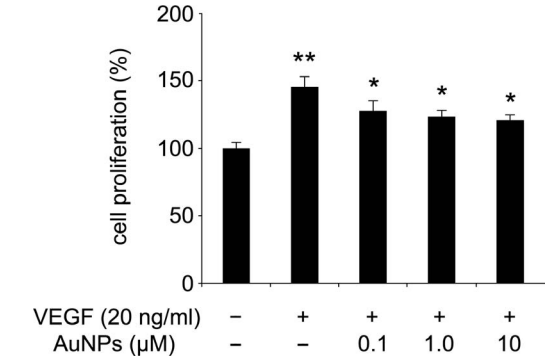

Figure 2. Gold nanoparticles suppress VEGF-induced endothelial cell proliferation. Human umbilical vein endothelial cells were pretreated with the indicated concentrations of AuNPs (0.1, 1.0, and 10 μM), followed by VEGF (20 ng/mL), and cell proliferation was tested with an MTT assay. Data represent the mean of three independent experiments. $^{**}P < 0.05$ versus basal cell proliferation (control); $^{*}P < 0.05$ versus VEGF-induced HUVEC proliferation.

Endothelial Cell Marker Staining Was Lower Within CNV Lesions With AuNP Treatment

Ninety-one (AuNP-treated mice) and 92 (PBS-treated mice) laser spots out of the respective 100 laser spots were evaluated for endothelial cell marker staining. Endothelial cells within laser-induced CNV lesions were labeled with isolectin B4, and the nuclei of RPE cells were stained with DAPI. Figure 6 demonstrates representative images of RPE–choroid flat mounts labeled with Alexa Fluor 568–conjugated isolectin B4 (left) and DAPI (middle), and the combined, merged image (right). The isolectin B4–labeled areas in the AuNP- and PBS-treated groups were 10,962.1 ± 7832.9 and 5243.9 ± 3811.8, respectively (arbitrary units). The extent of the isolectin B4–labeled area was much smaller in the AuNP-treated group than in the PBS-treated group ($P < 0.05$); the AuNP-treated group showed a 52.2% reduction in the isolectin B4–labeled area compared with the PBS-treated group.

Discussion

In the present study, we investigated whether intravitreal injection of AuNPs could inhibit laser-induced CNV in an experimental CNV mouse model. Gold nanoparticles inhibited the development of experimental CNV and suppressed ERK1/2, Akt, and FAK signaling pathways in HUVECs. In addition, without in vitro cellular toxicity, both VEGF-induced endothelial cell tube formation and proliferation were inhibited by AuNPs.

Although the exact mechanisms of the inhibitory effects of AuNPs on angiogenesis have not yet been fully elucidated, AuNPs have been reported to bind heparin-binding growth

Investigative Ophthalmology & Visual Science

Downloaded from iovs.arvojournals.org on 01/20/2022

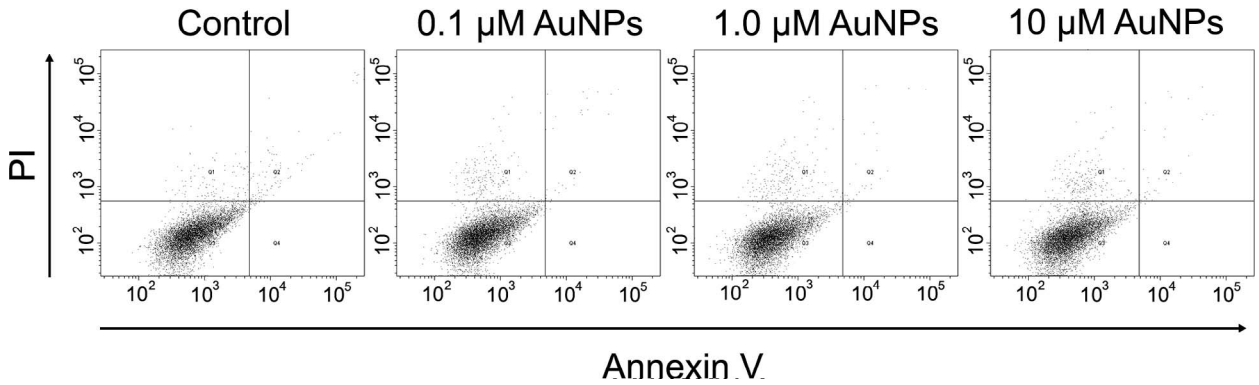

FIGURE 3. No ARPE-19 cytotoxicity was induced by AuNPs. ARPE-19 cells were treated with various concentration of AuNPs (0.1, 1.0, and 10 μM) and further incubated for 24 hours. Cell death was quantified by flow cytometry using PI and annexin V. Treatment with AuNPs did not significantly increase the proportion of PI-positive or annexin V–positive ARPE-19 cells.

factor through cysteine residues on the heparin-binding domain and inhibit its interaction with receptors, thereby exerting an antiangiogenic effect.[12,13] In the literature, AuNPs have unique physicochemical properties to bind selectively with amine and thiol groups, which exist in the cysteine side-chain. Therefore, AuNPs inhibit subsequent growth factor-mediated signaling activity.[18] Moreover, AuNPs can bind VEGF, basic fibroblast growth factor, and placental growth factor, resulting in inhibition of endothelial cell proliferation and VEGF-induced permeability.[19] Furthermore, it was recently reported that AuNPs significantly induces nonstructural reorganization of VEGFR-2[20] and inhibits VEGF-induced phosphorylation of VEGFR-2.[13] In the present study, RPE cells, which also play a critical role in AMD pathogenesis, were used for evaluating the cellular toxicity of AuNPs. Flow cytometric analysis showed no apoptotic or necrotic RPE cells even with the highest AuNP concentration tested.

According to previous studies in nanotoxicology, the most important factors that are likely to affect cytotoxicity of nanoparticles are size, concentration, and surface charge.[20,21] For AuNPs, these factors are also considered important for their cytotoxicity. When gold particles are larger than 5 nm, they are generally thought to be chemically inert. Pan et al.[20] showed that smaller AuNPs (<1.4 nm) were more toxic than their larger equivalents, and 1.4-nm AuNPs resulted in IC_{50} values ranging from 30 to 56 μM. However, 15-nm AuNPs were relatively nontoxic. Previous study also demonstrated that 20-nm AuNPs was nontoxic to retinal vascular endothelial cells and neural retinal tissue.[13] Surface charge of AuNPs affects cytotoxicity also. In the evaluation of effects of neural, anionic, and cationic AuNPs, cationic particles are moderately toxic, whereas anionic or neutral particles are quite nontoxic.[22] The surface charge and the size of AuNPs used in the present study are neutral and 20 nm, respectively. These characters may have led to the nontoxicity of AuNPs. These results also seem to support the previous toxicologic safety data for AuNPs.

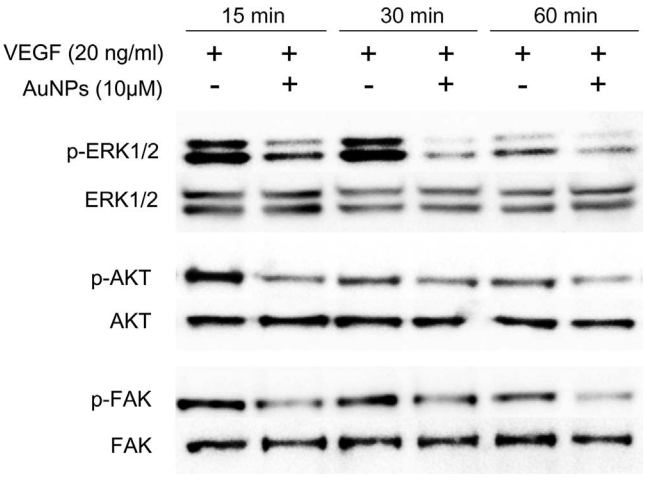

FIGURE 4. Gold nanoparticles inhibited the phosphorylation of ERK1/2, Akt, and FAK induced by VEGF. Human umbilical vein endothelial cells were pretreated with AuNPs (10 μm) for 2 hours, followed by VEGF (20 ng/mL) administration; cells were further incubated for the indicated time points (15, 30, and 60 minutes) and phosphorylated, and total ERK1/2, Akt, and FAK were analyzed by Western blot.

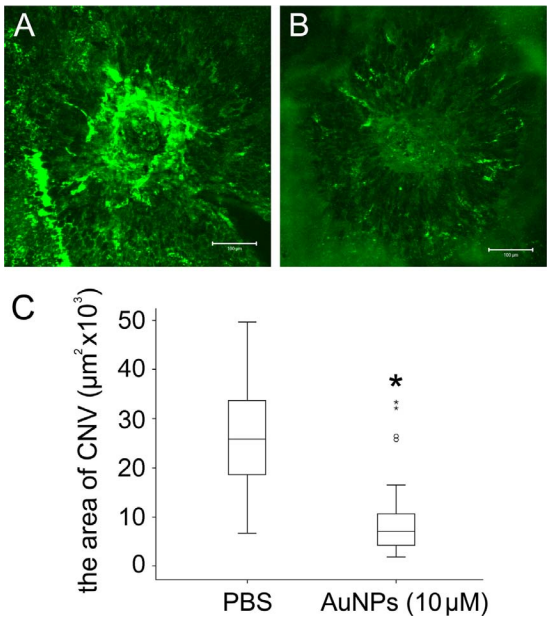

FIGURE 5. Gold nanoparticles suppressed the development of CNV in a laser-induced CNV model. Choroidal neovascularization lesions were labeled with fluorescein-labeled dextran 14 days after laser photocoagulation. (**A**) CNV image from intravitreal PBS-injected mouse eye (1 μL). (**B**) CNV image from an intravitreal AuNP-injected mouse eye (10 μM, 1 μL). *Scale bar* denotes100 μm in length. (**C**) Eyes treated with intravitreal AuNP injection showed smaller and less dense CNV formation compared with PBS-treated eyes. There is a significant difference between CNV size in PBS- and AuNP-injected eyes. *$P < 0.001$ versus CNV area in PBS-injected eyes.

Investigative Ophthalmology & Visual Science

Downloaded from iovs.arvojournals.org on 01/20/2022

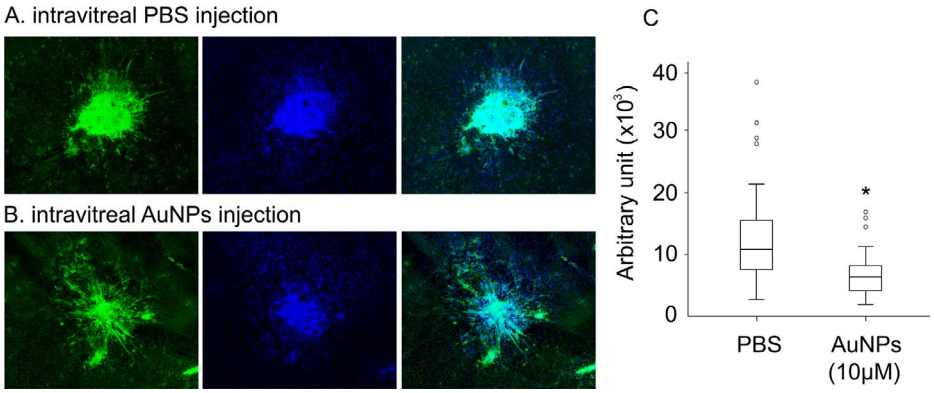

Figure 6. Gold nanoparticles decreased the immunofluorescent staining of isolectin B4, an endothelial cell marker. Immunofluorescence staining of laser-induced CNV 14 days after laser application. Retinal pigment epithelium–choroid preparations were fluorescently labeled with isolectin B4 (*green channel*) and the nuclear marker DAPI (*blue channel*). (**A**) Immunofluorescence staining of CNV lesion from an intravitreal PBS-injected mouse eye. (**B**) Immunofluorescence staining of a CNV lesion from an intravitreal AuNP-injected mouse eye. *Scale bar* denotes 100 μm in length. (**C**) Boxplot of the CNV area labeled with isolectin B4 in PBS- and AuNP-treated eyes. The size of the isolectin B4-labeled area (in arbitrary unit) in AuNP-treated eyes is much smaller compared with PBS-treated eyes. $^*P < 0.05$ versus CNV area in PBS-injected eyes.

Since the 1970s, gold-based compounds have been clinically used to treat patients with rheumatoid arthritis.[23] Gold compounds were applied to reduce inflammation and to slow disease progression primarily in patients that have a poor prognosis. Recently, nanoscale gold particles have shown great potential for diagnostic and therapeutic purposes in nanomedicine and are being actively investigated as drug carriers, photothermal agents, contrast agents, and radiosensitizers.[9] Given that VEGF plays a key role in the pathogenesis of CNV secondary to AMD, AuNPs themselves might be excellent therapeutic agents. Intravitreal injection of AuNPs could be applied into eyes with CNV to inhibit VEGF-mediated signaling.

Gold nanoparticles injected into the vitreous cavity can be easily seen how they are being dispersed in the vitreous body, because AuNPs are a ruby red–colored liquid. The ocular biodistribution of AuNPs can provide insight into the bioavailability, cellular uptake, duration of action, and toxicity. However, they are not well known. Nanoparticles are generally considered to be able to avoid the quick clearance and improve retention in the vitreous and the retina compared with large molecules.[24–27] The larger molecules are cleared from the vitreous body by the circulation and vitreous turnover, resulting in short intraocular half-life. Particle size-dependent ocular distribution and half-life were investigated in rabbits by Sakurai et al.[28] The 2-μm particles ($t_{1/2}$ = 5.4 days) were detected near trabecular meshwork where they were drained out, whereas the 200-nm particles ($t_{1/2}$ = 8.6 days) were evenly distributed in the vitreous cavity, and the 50-nm particles ($t_{1/2}$ = 10.1 days) crossed the retina and were found to remain in the retina even after 2 months. The ocular biodistribution of 20-nm AuNPs in mice after intravenous injection was reported.[29] The AuNPs passed through the blood–retinal barrier and were distributed in all retinal layers, including neurons, endothelial cells, and periendothelial glial cells. These cells did not show any structural abnormality and cytotoxicity. Although the intraocular kinetics of intravitreally injected 20-nm AuNPs is not known, the 20-nm AuNPs seem to be well tolerated in vitreous cavity and retina without retinal toxicity

Therapeutic strategies using AuNPs begin with analyzing the signaling cascades through which they control disease progression. In previous reports, a significant inhibitory effect of AuNPs on VEGF-induced VEGFR2 phosphorylation was demonstrated.[13] The signaling pathways investigated the present study, including ERK1/2, Akt, and FAK, play important roles during angiogenesis. Extracellular signal–regulated kinase 1/2 signaling is considered a very important VEGF/VEGFR-2 downstream signaling pathway.[30] This pathway regulates endothelial cell function via RAS-RAF-MEK-MAPK-ERK1/2 signaling. ESK 1/2 signaling has been implicated in endothelial cell proliferation,[31] survival,[32,33] and protection against apoptosis.[34] Akt plays a role in endothelial cell migration via the PI3K-Akt-eNOS axis. Akt signaling pathway activation also promotes endothelial cell survival through blocking proapoptotic Bad and caspase 9 activation.[35,36] Downstream FAK signaling is strongly implicated in endothelial cell migration and VEGF-induced cytoskeletal reorganization.[37] In the present study, the expression levels of VEGF-induced ERK1/2, Akt, and FAK phosphorylation were all suppressed by AuNPs.

In conclusion, we demonstrated herein that AuNPs can inhibit CNV in an experimental model and are sufficient to suppress VEGF-induced activation of ERK1/2, Akt, and FAK signaling in HUVECs. Gold nanoparticles showed no cytotoxicity against RPE cells. Further study to assess effects of AuNPs in CNV is warranted.

Acknowledgments

Supported by Clinical Research Institute grant CMCDJ-P-2013-24 funded by the Catholic University of Korea, Daejeon St. Mary's Hospital.

Disclosure: **Y.-J. Roh**, None; **C.R. Rho**, None; **W.-K. Cho**, None; **S. Kang**, None

References

1. Ferris FL III, Fine SL, Hyman L. Age-related macular degeneration and blindness due to neovascular maculopathy. *Arch Ophthalmol*. 1984;102:1640–1642.
2. Lee P, Wang CC, Adamis AP. Ocular neovascularization: an epidemiologic review. *Surv Ophthalmol*. 1998;43:245–269.
3. Ambati J, Ambati BK, Yoo SH, Ianchulev S, Adamis AP. Age-related macular degeneration: etiology, pathogenesis, and therapeutic strategies. *Surv Ophthalmol*. 2003;48:257–293.
4. Campochiaro PA. Molecular targets for retinal vascular diseases. *J Cell Physiol*. 2007;210:575–581.
5. Rosenfeld PJ, Brown DM, Heier JS, et al; MARINA Study Group. Ranibizumab for neovascular age-related macular degeneration. *N Engl J Med*. 2006;355:1419–1431.
6. Ishibashi T, Hata Y, Yoshikawa H, et al. Expression of vascular endothelial growth factor in experimental choroidal neovas-

Investigative Ophthalmology & Visual Science

Downloaded from iovs.arvojournals.org on 01/20/2022

cularization. *Graefes Arch Clin Exp Ophthalmol*. 1997;235: 159–167.

7. Millauer B, Wizigmann-Voos S, Schnürch H, et al. High affinity VEGF binding and developmental expression suggest Flk-1 as a major regulator of vasculogenesis and angiogenesis. *Cell*. 1993; 72:835–846.
8. Crawford Y, Ferrara N. VEGF inhibition: insights from preclinical and clinical studies. *Cell Tissue Res*. 2009;335: 261–269.
9. Arvizo R, Bhattacharya R, Mukherjee P. Gold nanoparticles: opportunities and challenges in nanomedicine. *Expert Opin Drug Deliv*. 2010;7:753–763.
10. Jeong EH, Jung G, Hong CA, Lee H. Gold nanoparticle (AuNP)-based drug delivery and molecular imaging for biomedical applications. *Arch Pharm Res*. 2014;37:53–59.
11. Liu X, Atwater M, Wang J, Huo Q. Extinction coefficient of gold nanoparticles with different sizes and different capping ligands. *Colloids Surf B Biointerfaces*. 2007;58:3–7.
12. Kemp MM, Kumar A, Mousa S, et al. Gold and silver nanoparticles conjugated with heparin derivative possess anti-angiogenesis properties. *Nanotechnology*. 2009;20:455104.
13. Kim JH, Kim MH, Jo DH, et al. The inhibition of retinal neovascularization by gold nanoparticles via suppression of VEGFR-2 activation. *Biomaterials*. 2011;32:1865–1871.
14. Kennedy LC, Bickford LR, Lewinski NA, et al. A new era for cancer treatment: gold-nanoparticle-mediated thermal therapies. *Small*. 2011;7:169–183.
15. Miura S, Matsuo Y, Saku K. Transactivation of KDR/Flk-1 by the B2 receptor induces tube formation in human coronary endothelial cells. *Hypertension*. 2003;41:1118–1123.
16. Kang S, Park KC, Yang KJ, et al. Effect of cediranib, an inhibitor of vascular endothelial growth factor receptor tyrosine kinase, in a mouse model of choroidal neovascularization. *Clin Experiment Ophthalmol*. 2013;41:63–72.
17. Kang S, Roh YJ, Kim IB. Antiangiogenic effects of tivozanib, an oral VEGF receptor tyrosine kinase inhibitor, on experimental choroidal neovascularization in mice. *Exp Eye Res*. 2013;112: 125–133.
18. Mukherjee P, Bhattacharya R, Wang P, et al. Antiangiogenic properties of gold nanoparticles. *Clin Cancer Res*. 2005;11: 3530–3534.
19. Arvizo RR, Rana S, Miranda OR, et al. Mechanism of anti-angiogenic property of gold nanoparticles: role of nanoparticle size and surface charge. *Nanomedicine*. 2011;7:580–587.
20. Pan Y, Ding H, Qin L, et al. Gold nanoparticles induce nanostructural reorganization of VEGFR2 to repress angiogenesis. *J Biomed Nanotechnol*. 2013;9:1746–1756.
21. Jo DH, Lee TG, Kim JH. Nanotechnology and nanotoxicology in retinopathy. *Int J Mol Sci*. 2011;12:8288–8301.
22. Goodman CM, McCusker CD, Yilmaz T, Rotello VM. Toxicity of gold nanoparticles functionalized with cationic and anionic side chains. *Bioconjug Chem*. 2004;15:897–900.
23. Currey HL, Harris J, Mason RM, et al. Comparison of azathioprine, cyclophosphamide, and gold in treatment of rheumatoid arthritis. *Br Med J*. 1974;3:763–766.
24. Shelke NB, Kadam R, Tyagi P, Rao VR, Kompella UB. Intravitreal poly(L-lactide) microparticles sustain retinal and choroidal delivery of TG-0054, a hydrophilic drug intended for neovascular diseases. *Drug Deliv Transl Res*. 2011;1:76–90.
25. Bakri SJ, Snyder MR, Reid JM, et al. Pharmacokinetics of intravitreal ranibizumab (Lucentis). *Ophthalmology* 2007;114: 2179–2182.
26. Gaudreault J, Fei D, Rusit J, et al. Preclinical pharmacokinetics of Ranibizumab (rhuFabV2) after a single intravitreal administration. *Invest Ophthalmol Vis Sci*. 2005;46:726–733.
27. Gupta SK, Velpandian T, Dhingra N, Jaiswal J. Intravitreal pharmacokinetics of plain and liposome-entrapped fluconazole in rabbit eyes. *J Ocul Pharmacol Ther*. 2000;16:511–518.
28. Sakurai E, Ozeki H, Kunou N, Ogura Y. Effect of particle size of polymeric nanospheres on intravitreal kinetics. *Ophthalmic Res*. 2001;33:31–36.
29. Kim JH, Kim JH, Kim KW, et al. Intravenously administered gold nanoparticles pass through the blood-retinal barrier depending on the particle size, and induce no retinal toxicity. *Nanotechnology*. 2009;20:505101.
30. Veikkola T, Karkkainen M, Claesson-Welsh L, Alitalo K. Regulation of angiogenesis via vascular endothelial growth factor receptors. *Cancer Res*. 2000;60:203–212.
31. Meadows KN, Bryant P, Pumiglia K. Vascular endothelial growth factor induction of the angiogenic phenotype requires Ras activation. *J Biol Chem*. 2001;276:49289–49298.
32. Berra E, Milanini J, Richard DE, et al. Signaling angiogenesis via p42/p44 MAP kinase and hypoxia. *Biochem Pharmacol*. 2000;60:1171–1178.
33. Gupta K, Kshirsagar S, Li W, et al. VEGF prevents apoptosis of human microvascular endothelial cells via opposing effects on MAPK/ERK and SAPK/JNK signaling. *Exp Cell Res*. 1999;247: 495–504.
34. Alavi A, Hood JD, Frausto R, et al. Role of Raf in vascular protection from distinct apoptotic stimuli. *Science*. 2003;301: 94–96.
35. Gerber HP, McMurtrey A, Kowalski J, et al. Vascular endothelial growth factor regulates endothelial cell survival through the phosphatidylinositol 3′-kinase/Akt signal transduction pathway. Requirement for Flk-1/KDR activation. *J Biol Chem*. 1998;273:30336–30343.
36. Gerber HP, Dixit V, Ferrara N. Vascular endothelial growth factor induces expression of the antiapoptotic proteins Bcl-2 and A1 in vascular endothelial cells. *J Biol Chem*. 1998;273: 13313–13316.
37. Lustig-Yariv O, Schulze E, Komitowski D, et al. The expression of the imprinted genes H19 and IGF-2 in choriocarcinoma cell lines. Is H19 a tumor suppressor gene? *Oncogene*. 1997;15: 169–177.

Investigative Ophthalmology & Visual Science

Downloaded from iovs.arvojournals.org on 01/20/2022